Korean J. Chem. Eng., 38(2), 264-275 (2021)
DOI: 10.1007/s11814-020-0717-9

pISSN: 0256-1115
eISSN: 1975-7220

A breakage model with different liquid properties for pressurized bubble columns in a homogeneous regime

Bay Van Tran*, Son Ich Ngo*, Young-Il Lim*,†, Kang-Seok Go, and Nam-Sun Nho****

*Center of Sustainable Process Engineering (CoSPE), Department of Chemical Engineering, Hankyong National University, Jungang-ro 327, Anseong-si, Gyeonggi-do 17579 Korea
**Center for Convergent Chemical Process (CCP), 141 Gajeong-ro, Yuseong-gu, Daejeon 34114, Korea
(*Received 21 June 2020 • Revised 8 October 2020 • Accepted 22 November 2020*)

Abstract−The bubble breakage rate in gas-liquid bubble columns increases for organic liquid and at high pressure. This study developed a breakage model that accounts for different liquid properties in gas-liquid pressurized bubble columns in the homogeneous regime. The Luo (1996), Lehr (2002), and Wang (2003) breakage models, which are widely used for the population balance equation (PBE) of bubble columns, were compared in terms of the total breakage rate, daughter size distribution, and computational time. The model with two empirical equations, modified from Luo's breakage kernel, was proposed. One represented bubble deformation behavior in different liquid properties in terms of buoyancy, surface tension, and viscosity. The other considered the effect of operating pressure (or gas density) on the breakage rate. The modified model was compared with experimental data and a rigorous breakage model from the literature. The proposed breakage model shows good agreement with experimental data and computational efficiency. This breakage model is applicable for computational fluid dynamics with PBE in pressurized bubble columns with organic liquids.

Keywords: Bubble Column, Breakage Model, Homogeneous Regime, Organic Liquid, High Pressure Operation

INTRODUCTION

Bubble columns in which the gas phase is dispersed into a liquid or liquid-solid continuous phase are widely used in the chemical, petrochemical [1], biological [2], and pharmaceutical industries because of their good mixing, high mass and heat transfer rates [3-5], and low operating cost [6]. Industrial bubble columns are used with highly viscous liquids or concentrated slurries [7] at high temperature and pressure for applications such as hydrocracking of petroleum residue (5-21 MPa), coal liquefaction (17 MPa), Fischer-Tropsch synthesis (1-5 MPa), benzene hydrogenation (5 MPa), and oxidation of paraxylene to terephthalic acid (0.3-3 MPa) [8-10].

Depending on the superficial gas velocity and column diameter, the flow regime inside the bubble column can be classified into homogeneous, transitional, or heterogeneous flow [3,11]. Catalytic hydrocracking of heavy residues proceeds in the homogeneous regime to reduce coke formation [1,12]. The Fischer-Tropsch bubble column is often operated at high gas velocity in the heterogeneous regime [6,13]. Even in the homogeneous flow regime, the bubble size and shape changes along the column height [11,14] and the bubble size is dispersed with the spherical and ellipsoidal shapes due to breakage and coalescence [11].

Fundamental parameters, such as the gas holdup, bubble size distribution (BSD), interfacial area, and liquid mass transfer coefficient, are essential for the scale-up and design of bubble columns [1,8,15]. The population balance model (PBM) including breakage and coalescence of bubbles was used to identify the BSD of bubble columns [1,16]. Computational fluid dynamics (CFD) models coupled with PBM were applied to investigate both the gas holdup and bubble size in bubble columns [1,17,18].

Many researchers have developed breakage models, considering turbulent eddies [4,5,19], liquid properties [17,20], and operating pressures [21,22]. The Luo model assumes that the bubbles will break-up if the turbulent kinetic energy of bombarding eddies exceeds a critical value [19]. The Lehr model considers that the bubbles will break-up if the turbulent inertial stress of the bombarding eddies exceeds the interfacial surface restoring stress of the smallest daughter size [4]. The Wang model combines both the Luo and Lehr criteria for the breakup mechanism [5].

Most breakage models are based on an energy criterion represented by (1) the surface energy of mother bubbles [23], (2) the increase in surface energy before and after breakage [5,19], or (3) the mean value of the surface energy increase for breakage into two equal-sized daughter bubbles and a non-equal-sized daughter bubble [24]. However, none of the bubble breakage models have managed to capture the mechanisms of energy transfer between bubbles and bombarding eddies [25]. Therefore, the existing breakage models must be improved to bridge the gap between the ideal to realistic breakage.

Organic liquid properties, such as density, viscosity, and surface tension, influence the hydrodynamics, bubble breakup, and coalescence in the bubble column [1,17,26]. The bubble column hydrodynamics for different inorganic and organic liquids, such as water, toluene, and ligroin, have been predicted [17] using the Wang break-

†To whom correspondence should be addressed.
E-mail: limyi@hknu.ac.kr

age model [5]. However, the Wang model is computationally prohibitive [25]. When the breakage model within the PBM is integrated into CFD simulation in a two- or three-dimensional (2D or 3D) geometry, the development of a fast and robust breakage kernel is necessary.

The effect of pressure (or gas density) on the hydrodynamics of bubble columns has been investigated because industrial bubble columns are generally operated at high pressure [7]. The increase in pressure forces bubbles to break into smaller bubbles [7]. Considering the internal flow through the bubble neck, a three-step breakup mechanism was presented to capture the effect of pressure on the breakup rate and daughter size distribution [9]. Recently, the Xing model was improved by adequately describing the flow inside a deformed bubble via static stress analysis, interfacial stress of the bubble neck, and viscous flow resistance [20]. Although the Zhang breakage model [20] has been applied to a wide range of flow regimes under high pressures, there is little evidence for the homogeneous regime and computational efficiency. A breakage model with pressure correction factors was proposed to predict hydrodynamics of a homogeneous bubble column under elevated pressure [1], which was applicable only to the air-water system. Therefore, there remains a need for a computationally-efficient breakage model suitable for high pressures and organic liquids.

The aim of this study was to develop an efficient breakage model applicable to the homogeneous flow regime in the pressurized bubble column for a wide range of liquid properties. The breakage models, including the Luo, Lehr, and Wang models, are compared with experimental data available in the literature to address their advantages and drawbacks. A novel breakage model that takes into account the operating pressure and liquid properties is proposed for the homogeneous regime in bubble columns.

BUBBLE BREAKAGE MODEL

For bubble columns, the PBM describes the evolution of a bubble density function that represents the birth and death of bubbles due to coalescence and breakage. The bubble breakage process requires knowledge of the breakage rate and daughter size distribution. The three existing breakage models [4,5,19], called the Luo, Lehr, and Wang models, are first presented to state the necessity of a new breakage model for various liquids and pressures in the homogeneous regime. The existing models are then compared in terms of the breakage rate (Ω), daughter size distribution (β), and computational time. Finally, a modified breakage model based on the Luo model is proposed and validated with experimental data and rigorous models.

1. Luo, Lehr, and Wang Breakage Models

The Luo, Lehr, and Wang breakage models were established under the following common assumptions: (1) the breakup takes place due to turbulence; (2) the breakup is caused by arriving eddies of different length scales with the size equal to or smaller than the bubble size onto the surface of the bubbles; (3) the theory of isotropic turbulence is adopted in the calculation of collision frequency; (4) only the binary breakup into two daughter bubbles is considered; and (5) the bubble shape is spherical.

Table 1 compares the three breakage models with different breakup mechanisms. All the symbols in Table 1 are defined in the Nomenclature. According to probability theory, the Luo model implies that the probability (P_b) of a bubble with size d breaking up into size $f_v^{1/3}d$, when hit by an arriving eddy of size λ, is equal to the probability (P_e) of the arriving eddy of size λ with turbulent kinetic energy (e_λ) greater than or equal to the minimum kinetic energy required for the breakup ($e_{\lambda,crit}$) [19]. Based on the balance between the interfacial force of the bubble surface and the inertial force of the colliding eddy, the Lehr model assumes that immediately before the breakage, bubbles are locally nearly cylindrical, and therefore broken when the turbulent inertial stress of arriving eddy ($\frac{1}{2}\rho_l u_\lambda^2$) is greater than the interface restoring stress of the smallest daughter size ($\frac{2\sigma}{d'}$) [4]. The Wang model combines the two previous breakup constraints under the additional assumption that an eddy with size λ has an energy spectrum due to its turbulent motion [5]. Although the Wang model captures the two breakup mechanisms from the Luo and Lehr models, it requires an additional integral for the calculation of breakup probability and a nonlinear solver to find the maximum breakup fraction ($f_{v,max}$).

The total breakage rate (Ω, $1/m^3/s$) of the three models in Eq. (T1) was obtained from the breakage rate kernel (Ω_k) calculated from the breakage probability (P_b) and collision frequency (ω_λ) of arriving eddies on the surface of the bubble [19]. The breakup probability (P_b) can be solved as an algebraic function of $e_{\lambda,crit}$ and the mean kinetic energy ($\bar{e}_\lambda$), as indicated in Eqs. (T2) and (T3). However, one additional integral is needed to calculate P_b in Eq. (T4), as mentioned previously. Thus, to calculate Ω the Wang model requires triple integrals instead of the double integrals in the Luo and Lehr models.

Since ω_λ represents the number of collisions between a bubble with volume $\pi d^3/6$ and an eddy with size λ, the ω_λ is defined in Eq. T by an analogy with the kinetic theory of gas. Assuming isotropic turbulence on the length scale of the bubbles, the mean turbulent velocity ($\bar{u}_\lambda$) of eddies with size λ and dissipation rate ε is in Eq. (T5):

$$u_\lambda = \sqrt{2}(\varepsilon\lambda)^{1/3} \tag{1}$$

The number density of eddies (n_λ) based on the energy spectrum analysis and the relationship between the wave number and eddy size was calculated only in the liquid phase ($1-\alpha_g$) for the Luo and Wang models, while a constant n_λ for each eddy size λ was used for the Lehr model.

When a bubble with size d breaks into two bubbles, one with a size of $f_v^{1/3}d$ and the other with a size of $(1-f_v^{1/3})d$ are created in the binary breakup. The daughter size distribution $\beta(f_v, \lambda, e_\lambda)$ is calculated by the ratio of $\Omega_k(\lambda, e_\lambda)$ to $\Omega(f_v, \lambda, e_\lambda)$ in Eq. (T6).

2. Total Breakage Rates of Luo, Lehr, and Wang Models

For an air-water system in the homogeneous regime (ρ_g=1.2 kg/m^3, ρ_l=1,000 kg/m^3, σ=0.072 N/m, and ε=2 m^2/s^3), the breakage frequency (Ω_f, 1/s) of the three breakage models are compared with two sets of experimental data [8,27] for a single bubble (α_g=0, and n=$1/m^3$) in Fig. 1.

$$\Omega_f = \Omega/[(1-\alpha_g)n] \tag{2}$$

Table 1. Luo, Lehr, and Wang breakage models

Model	Luo	Lehr	Wang
Assumption	- The breakage volume fraction is stochastic (Maxwell distribution)	- The length scale of eddy is larger than a smaller bubble size (d′) after breakage.	- The eddy has an energy spectrum. - Stochastic breakage volume fraction
Breakage criteria	Turbulent kinetic energy of the arriving eddy is greater than a critical value: $P_b(f_v\|d, \lambda)=P_e[e_\lambda \geq e_{\lambda, crit}]$ $\lambda_{min} \leq \lambda \leq d$ $\lambda_{min}=(11.4\sim31.4)\,\nu_l^{3/4}/\varepsilon^{1/4}$	Turbulent inertial stress of the arriving eddy is greater than interfacial surface restoring stress of smallest daughter size (d′): $\frac{1}{2}\rho_l u_\lambda^2 \geq \frac{2\sigma}{d'}$, $d' \leq \lambda \leq d$	Dynamic pressure of turbulent eddy is larger than the capillary pressure, and the eddy kinetic energy is larger than the increment of the surface energy: $P_b(f_v\|d, \lambda)=P_e[e_\lambda \geq e_{\lambda, crit}]$ $\frac{1}{2}\rho_l u_\lambda^2 \geq \frac{2\sigma}{d'}$, $\lambda_{min} \leq \lambda \leq d$ $\lambda_{min}=(11.4\sim31.4)\,\nu_l^{3/4}/\varepsilon^{1/4}$
Total breakage rate ($1/m^3/s$)	$\Omega(f_v, \lambda, e_\lambda)=\int_0^{0.5}\Omega_k(\lambda, e_\lambda)df_v$, where $\Omega_k(\lambda, e_\lambda)=\int_{\lambda_{min}}^{d}\int_{e_{\lambda, crit}}^{\infty}P_b(f_v, \lambda, e_\lambda)\omega_\lambda(d)de_\lambda d\lambda$ (T1)		
Breakage probability	$\int_{e_{\lambda, crit}}^{\infty}P_b(f_v, \lambda, e_\lambda)de_\lambda=$ $\exp\left(-\frac{e_{\lambda, crit}}{\bar{e}_\lambda}\right)$ (T2) where $e_{\lambda, crit}=c_f\pi d^2\sigma$, $c_f=f_v^{2/3}+(1-f_v)^{2/3}-1$, $\bar{e}_\lambda=\frac{1}{2}\rho_l\frac{\pi}{6}\lambda^3\bar{u}_\lambda^2$, $\bar{u}_\lambda=\sqrt{2}(\varepsilon\lambda)^{1/3}$	$\int_{e_{\lambda, crit}}^{\infty}P_b(f_v, \lambda, e_\lambda)de_\lambda=$ $\frac{4\sigma}{\pi\rho_l\varepsilon^{2/3}\lambda^{2/3}d'}\exp\left(-\frac{e_{\lambda, crit}}{\bar{e}_\lambda}\right)$ (T3) where $e_{\lambda, crit}=\frac{1}{2}\rho_l\frac{\pi}{6}\lambda^3 u_{\lambda, crit}^2$, $u_{\lambda, crit}=\sqrt{\frac{We_{crit}\sigma}{d'}}$, $\bar{e}_\lambda=\frac{1}{2}\rho_l\frac{\pi}{6}\lambda^3\bar{u}_\lambda^2$, $\bar{u}_\lambda=\sqrt{2}(\varepsilon\lambda)^{1/3}$	$\int_{e_{\lambda, crit}}^{\infty}P_b(f_v, \lambda, e_\lambda)de_\lambda=$ $\int_{e_{\lambda, crit}}^{\infty}C_{f_v}\frac{1}{\bar{e}_\lambda}\exp(-e_\lambda/\bar{e}_\lambda)de_\lambda$ (T4) where $C_{f_v}=$ $\begin{cases}\frac{1}{f_{v, max}-f_{v, min}}, & f_{v, min}<f_v<f_{v, max},\\ 0 & else\end{cases}$ $e_{\lambda, crit}=\max\left(c_{f, max}\pi d^2\sigma, \frac{6f_{v, min}^{1/3}d}{\pi\lambda^3\sigma}\right)$, $\bar{e}_\lambda=\frac{1}{2}\rho_l\frac{\pi}{6}\lambda^3\bar{u}_\lambda^2$, $\bar{u}_\lambda=\sqrt{2}(\varepsilon\lambda)^{1/3}$, $c_{f, max}=\min\left(2^{1/3}-1, \frac{e_\lambda}{\pi d^2\sigma}\right)$, $f_{v, max}^{2/3}+(1-f_{v, max})^{2/3}-1=c_{f, max}$, $f_{v, min}=\left(\frac{\pi\lambda^3\sigma}{6e_\lambda d}\right)^3$
Collision frequency	$\omega_\lambda(d)=\frac{\pi}{4}(d+\lambda)^2\bar{u}_\lambda n_\lambda n$ where $n_\lambda=\frac{0.822(1-\alpha_g)}{\lambda^4}$	$\omega_\lambda(d)=\frac{\pi}{4}(d+\lambda)^2\bar{u}_\lambda n_\lambda n$ where $n_\lambda=\frac{0.8413}{\lambda^4}$	$\omega_\lambda(d)=\frac{\pi}{4}(d+\lambda)^2\bar{u}_\lambda n_\lambda n$ (T5) where $n_\lambda=\frac{0.822(1-\alpha_g)}{\lambda^4}$
Daughter size distribution	$\beta(f_v, \lambda, e_\lambda)=\frac{\Omega_k(\lambda, e_\lambda)}{\Omega(f_v, \lambda, e_\lambda)}$ (T6)		

A critical Weber number (We_{crit}) of 2.3 was chosen in the Lehr model [25]. To convert the breakup fraction of bubbles into experimentally measured Ω [8], the breakup time t_b is calculated as [28]:

$$t_b=c\frac{d^{2/3}}{\varepsilon^{1/3}} \quad (3)$$

where c is an empirical parameter. The breakup time for an air-water system was approximately 3.4-3.8 ms according to an experimental study [29], whereas the breakup time for liquid-liquid systems ranged from 4 to 10 ms [28]. Using c=1/8, the breakup time calculated by Eq. (3) for 1 mm≤d≤15 mm and ε=2 m^2/s^3 ranged from 2.7 to 4.5 ms, which agrees well with the experimental data [29].

The breakage frequencies obtained from the three breakage models are considerably lower than experimental data for d≤4 mm [27]. The breakage frequencies of the Luo and Wang models increased with the increase in bubble diameter (d), which coincides with experimental data for d>4 mm [8]. The Wang model provides the best predictions for a wide range of bubble sizes.

3. Daughter Size Distribution of Luo, Lehr, and Wang Models

The daughter size distributions (β) obtained from the three break-

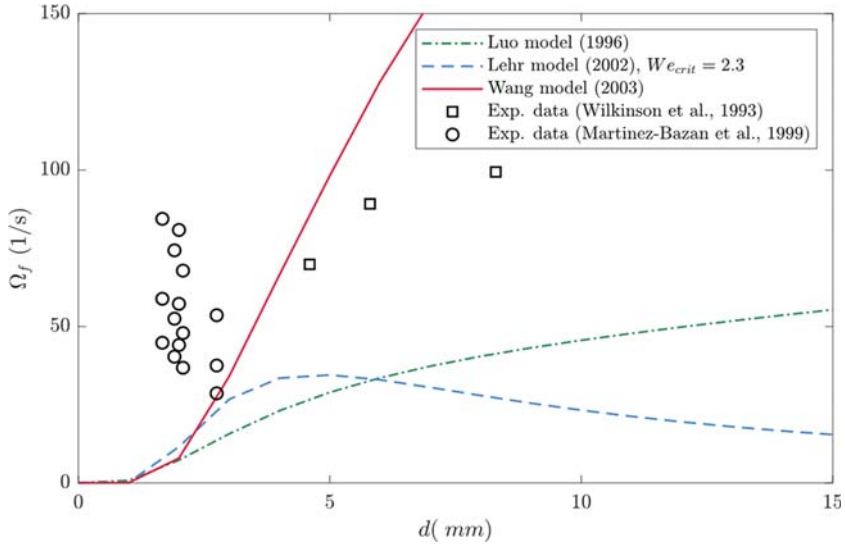

Fig. 1. Comparison of breakage frequency (Ω_f) with respect to bubble size (d) for air-water system.

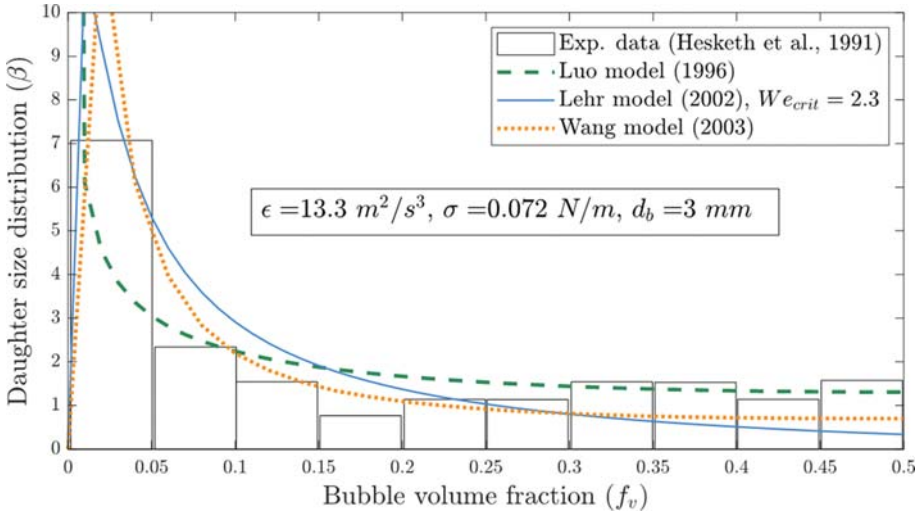

Fig. 2. Comparison of daughter size distributions (β) with respect to bubble volume fraction (f_v) for air-water system [30].

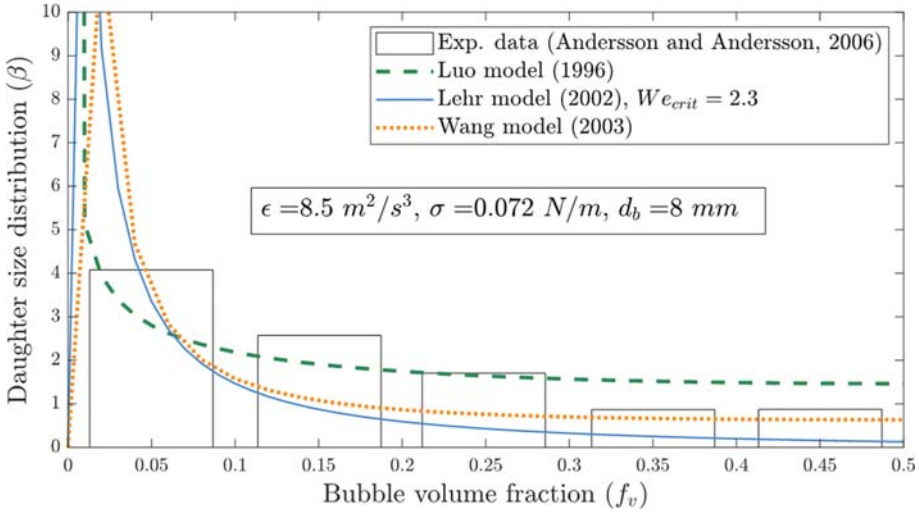

Fig. 3. Comparison of daughter size distributions (β) with respect to bubble volume fraction (f_v) for air-water system [29].

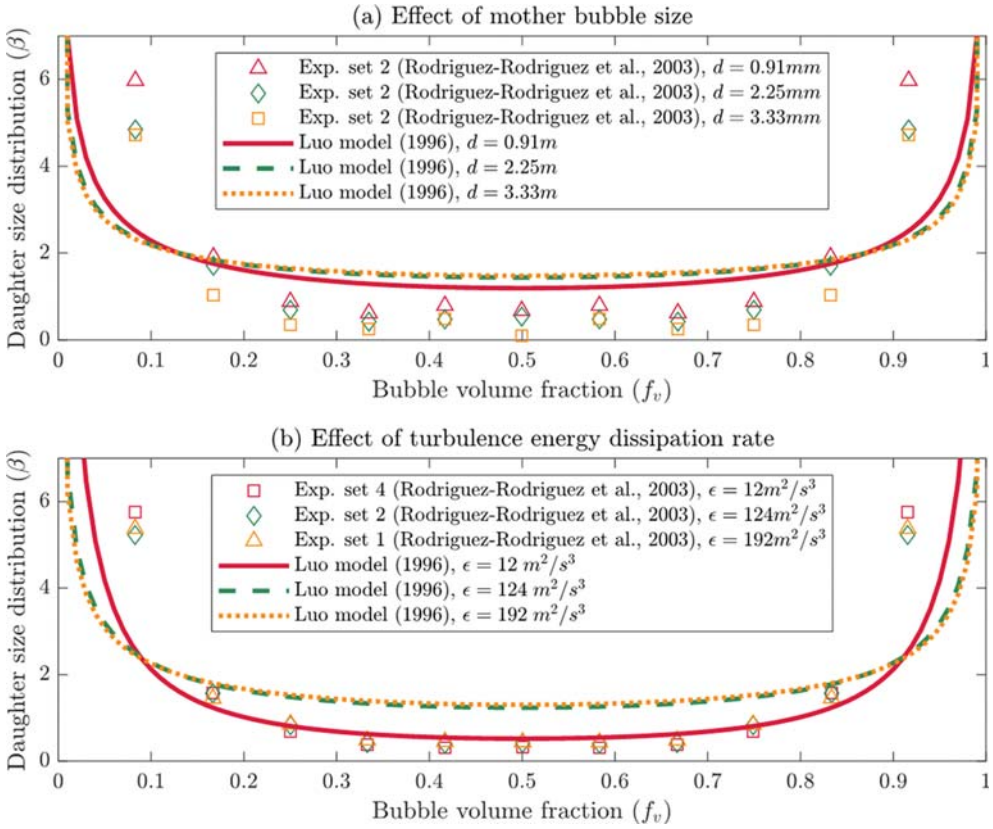

Fig. 4. Comparison of daughter size distribution (β) between experimental data [31] and the Luo model (1996).

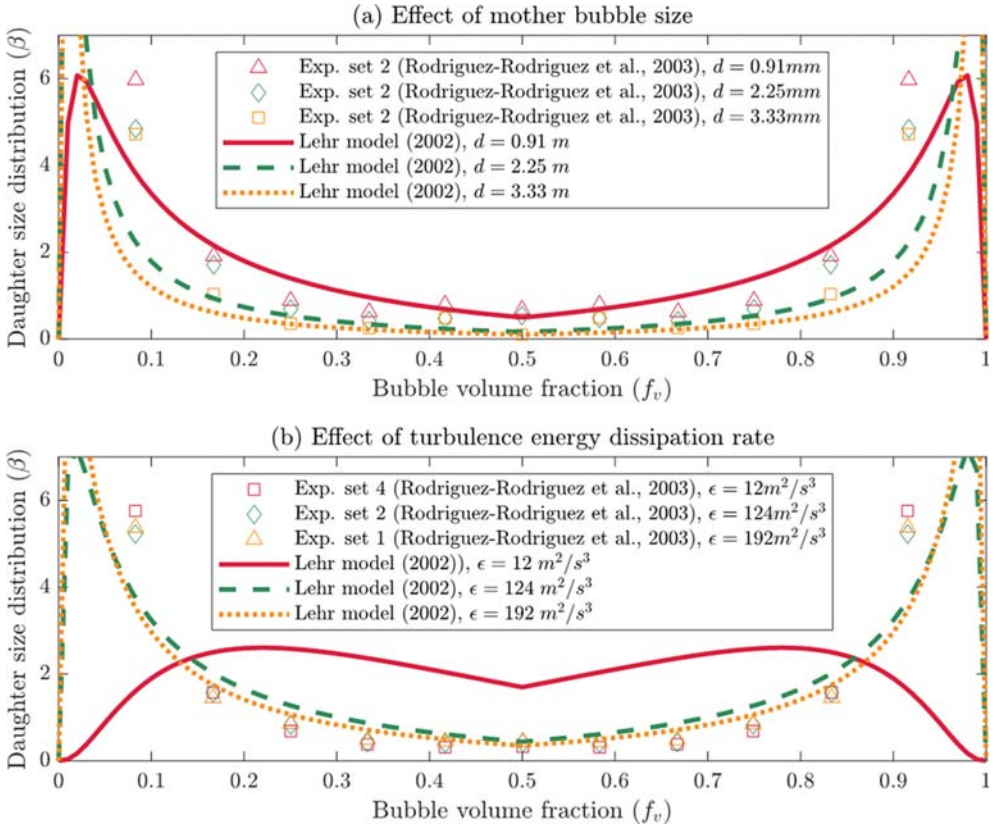

Fig. 5. Comparison of daughter size distribution (β) between experimental data [31] and the Lehr model (2002).

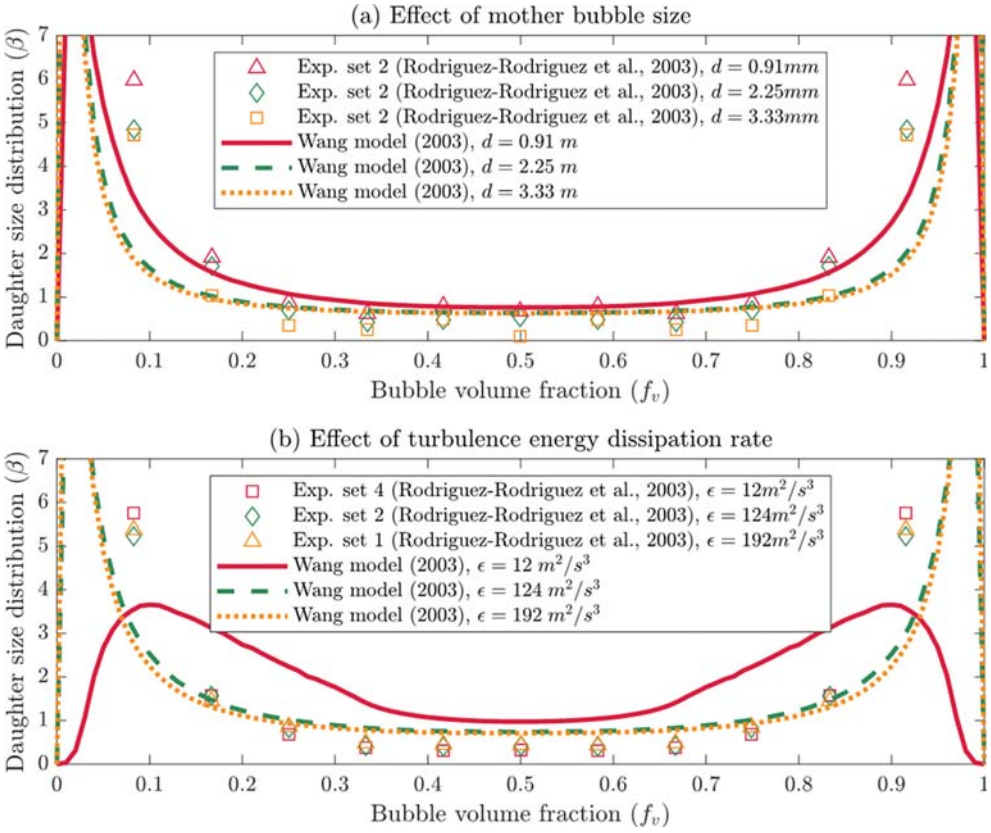

Fig. 6. Comparison of daughter size distribution (β) between experimental data [31] and the Wang model (2003).

age models were compared with experimental data for air-water systems [29,30] in Figs. 2 and 3. The experiment in Fig. 2 [30] was performed with a higher turbulence energy dissipation rate (ε= 13.3 m^2/s^3) and lower mother bubble size (d=3 mm) than that of Fig. 3 [29]. The daughter size distribution predicted from the three breakage models is comparable to the two sets of experimental data. The Luo model shows lower unequal-size breakup distribution (f_v≈0.05) and higher equal-size breakup distribution (f_v≈0.5) than the Lehr model. The results of the Wang model fall between those of the Luo and Lehr models.

The effects of the mother bubble size (d) at ε=124 m^2/s^3 and the turbulence energy dissipation rate (ε) at d=1 mm on β for the Luo, Lehr, and Wang models are compared with experimental data [31] in Figs. 4, 5, and 6, respectively. As shown in Figs. 4(a), 5(a), and 6(a), β values obtained from the Lehr and Wang models at high ε (=124 m^2/s^3) are closer to experimental dataset 2 than that from the Luo model. It was experimentally observed that the equal-size breakup fraction (f_v=0.5) slightly decreased with the increase in mother bubble size, which is the same tendency as the Lehr model (see Fig. 5(a)). The β values of the Luo and Wang models were not sensitive to d (see Figs. 4(a) and 6(a)). The tendency of the equal-size breakup fraction of the Luo model is opposite to that of experimental observations (see Fig. 4(a)). However, the Luo model provides more accurate predictions at low turbulent dissipation rate (ε=12 m^2/s^3) than the Lehr and Wang models (see Figs. 4(b), 5(b) and 6(b)).

The experimental data in Fig. 4(b) shows that the turbulence energy dissipation rate (ε) has little influence on β, and the equal-size breakup fraction (f_v=0.5) slightly increased with the increase in ε. The equal-size breakup fraction of the Luo model has a similar trend as the experimental observations (see Fig. 4(b)). However, the reversed trends were obtained from the Lehr and Wang models (see Figs. 5(b) and 6(b)). It is noted that the Lehr and Wang models are more favorable for the turbulent regime than the Luo model, whereas the Luo model performs better in the homogeneous flow regime.

4. Computational Time of Luo, Lehr, and Wang Models

Using the same numerical method (Gauss-Kronrod quadrature (quadgk)) [32] for the integrals in Matlab R2018 (Mathworks, Inc., Natick, USA) with four parallelized cores (2.3 GHz and 128 GB RAM), the computational times of the three breakage methods are listed in Table 2. The computational time was measured for the calculation of Ω and β from Eqs. (T1) to (T6) at ε=2 m^2/s^3 and 1≤d≤15 mm with 1 mm increment in the air-water system. The calculation times of the Lehr and Wang models are approximately 2 and 250 times, respectively, higher than that of the Luo model.

Table 2. Comparison of computational time between Luo, Lehr, and Wang models

Breakage model	Computational time (s)
Luo model [19]	0.18
Lehr model [4]	0.44
Wang model [5]	46.60

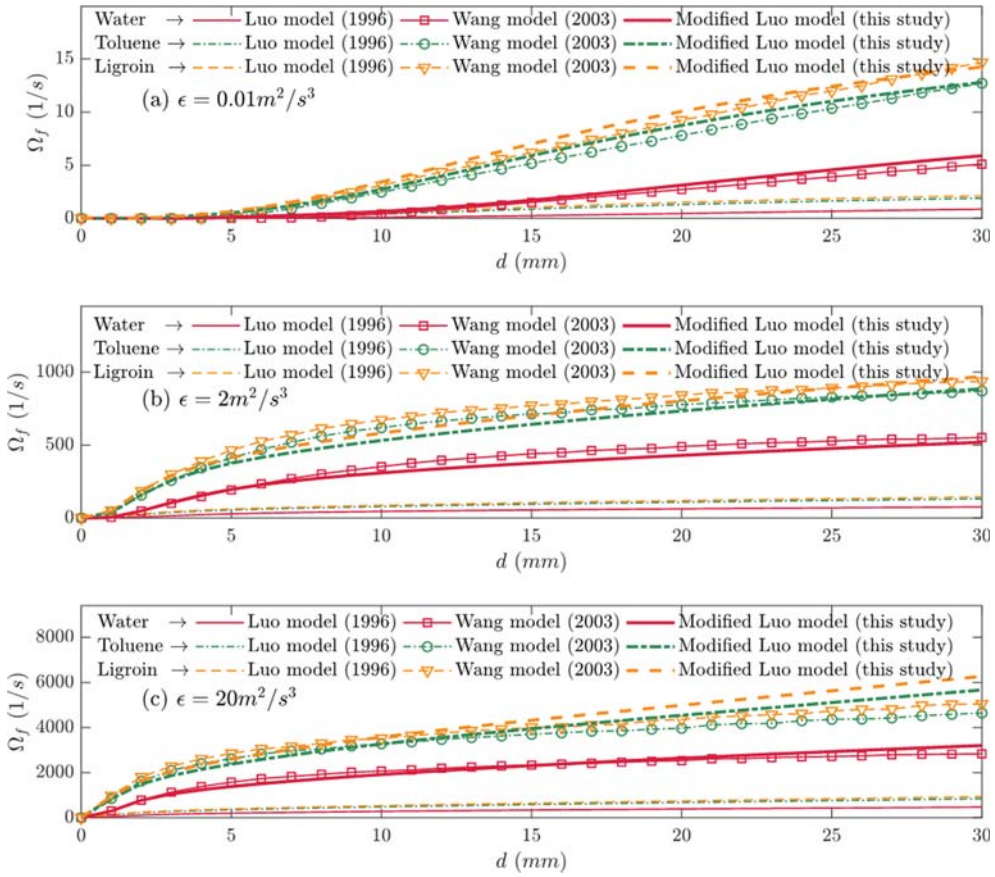

Fig. 7. Comparison of breakup frequency (Ω_f) obtained from the Luo, Wang, and modified Luo breakage models for water, toluene, and ligroin.

The difference in computational time is attributed to the calculation of the breakage probability in Eqs. (T2)-(T4). Since Eq. (T4) for the Wang model contains one additional integral, its computing time is much longer than that of the others. The Luo model has an advantage in terms of computing time if implemented in CFD-PBM simulation with a 2D or 3D geometry.

5. Modified Luo Model with Different Liquid Properties under High Pressure

The Luo breakage model is a good candidate for the homogeneous regime with low turbulence energy dissipation rates, compared with the Lehr and Wang models in terms of the breakup rate, daughter size distribution, and computing time. However, the Luo model is only valid for the air-water system at ambient pressure.

The Wang breakage model (Ω^W) has been validated for both water and organic liquids with low viscosity and surface tension in CFD-PBM simulation [5,17]. In the present study, instead of using the prohibitive Wang model, a modified Luo model that can be used for a wide range of liquid properties is proposed. Since the most important factors influencing bubble formation are buoyancy ($\rho_l - \rho_g$), surface tension (σ), and viscosity (μ_l) [33], which are represented by the Morton number (Mo), the Luo model (Ω^L) is modified with Mo:

$$\mathrm{Mo} = \frac{\mu_l^4 g(\rho_l - \rho_g)}{\rho_l^2 \sigma^3} \tag{4}$$

$$\Omega^{ML}(f_v, \lambda, e_\lambda) = \int_0^{0.5} \Omega_k^{ML}(\lambda, e_\lambda) df_v,$$

$$\text{where } \Omega_k^{ML}(\lambda, e_\lambda) = f(\mathrm{Mo}) \cdot \Omega_k^L(\lambda, e_\lambda) \tag{5}$$

The correction factor f(Mo) is proposed as the follows:

$$f(\mathrm{Mo}) = k_{M,1}(\mathrm{Mo})^{k_{M,2}} \tag{6}$$

To specify $k_{M,1}$ and $k_{M,2}$ in Eq. (6), the breakup frequency (Ω_f) was generated for 30 bubble sizes ($0 \le d_b \le 30$ mm) and 65 dissipation rates ($0 \le \varepsilon \le 2$ m^2/s^3). The total data points were 1950 for each type of liquid. Minimizing the error between the Wang model (Ω^W) and modified Luo model (Ω^{ML}) for three liquid systems (water, toluene, and ligroin), the $k_{M,1}$ and $k_{M,2}$ were estimated to be 4.9928 and −0.0126, respectively.

Fig. 7 compares the breakage frequency (Ω_f) of water, toluene, and ligroin at relatively low turbulence energy dissipation rates (ε= 0.01, 2, and 20 m^2/s^3), which were obtained from the Luo, Wang, and modified Luo models. The original Luo model (Ω^L) shows relatively low breakup rates compared with the Wang model. The modified Luo model (Ω^{ML}) accurately follows the Wang model at ε=0.01 and 2 m^2/s^3, as shown in Figs. 7(a) and 7(b). At ε=20 m^2/s^3, Ω^{ML} deviates slightly from Ω^W for toluene (σ=0.0204 N/m) and ligroin (σ=0.0283 N/m), as shown in Fig. 7(c). Eq. (6) is valid in the ranges $0.0204 \le \sigma \le 0.0727$ N/m, $0.47 \le \mu_l \le 1.07$ mPa·s, and $714 \le \rho_l \le 1{,}000$ kg/^{3} at relatively low turbulence energy dissipation rate.

The gas density correction factor was applied to Eq. (5) to con-

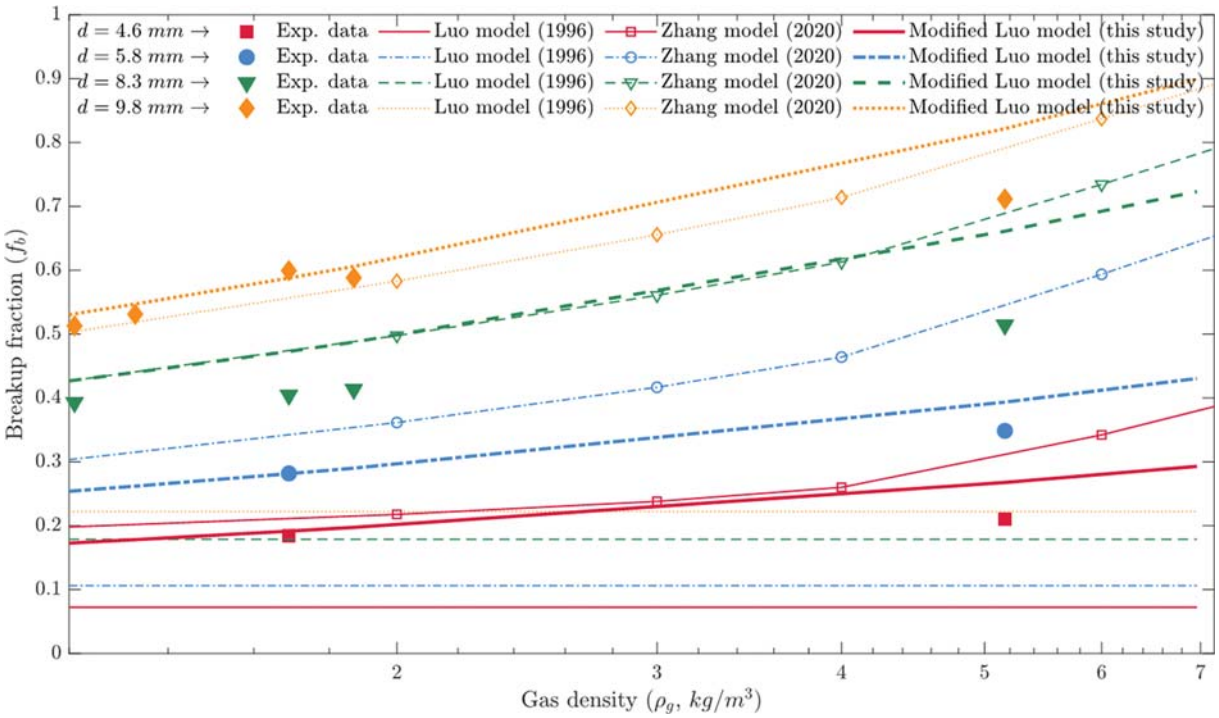

Fig. 8. Comparison of bubble breakup fractions (f_b) obtained from the Luo, Zhang, and modified Luo breakage models with experimental data for different bubble diameters.

sider the effect of pressure (or gas density) on the breakup rate, which is analogous to the pressure correction factors [1,22].

$$\Omega_k^{ML}(\lambda, e_\lambda) = k_{P1}\left(\frac{\rho_g}{\rho_{g,0}}\right)^{k_{P2}} \cdot f(Mo) \cdot \Omega_k^{L}(\lambda, e_\lambda) \tag{7}$$

where $\rho_{g,0}$ (=1.2 kg/m^3) is the air density under ambient condition; and k_{P1} and k_{P2} are the gas density correction factors estimated from experimental data for different gas densities and single bubble sizes [8]. The bubble breakup fractions (f_b) were measured in the experiment and were calculated from Ω^L, Ω^Z, and Ω^{ML} in the following equation:

$$f_b = \frac{t_b \Omega}{(1-\alpha_g)n} \tag{8}$$

Replacing Ω in Eq. (8) by $\Omega_k^{ML}(\lambda, e_\lambda)$ in Eq. (7) and minimizing the error of f_b between Eq. (8) and 25 experimental data [8], k_{P1}= 0.35 and k_{P2}=0.3 were obtained in the range of $1.2 \le \rho_g \le 7.0$ kg/m^3.

Fig. 8 compares the bubble breakup fractions (f_b) according to the gas density (ρ_g), which were obtained from the Luo model (Ω^L), Zhang model (Ω^Z), and modified Luo model (Ω^{ML}), with the experimental data [8]. A rigorous breakage model (Ω^Z) was recently proposed by Zhang et al. (2020) that considers the effect of dynamic pressure on the internal flow through the bubble neck [20].

The original Luo model (Ω^L) does not change with gas density and gives low f_b compared with the experimental data. The modified Luo model (Ω^{ML}) is a better fit to the experimental data than the Zhang model (Ω^Z). The Ω^{ML} in Eq. (7) does not change the daughter size distribution (β) in Eq. (T6), whereas it increases the breakage rate (Ω_k) in Eq. (T1).

VALIDATION AND EVALUATION OF MODIFIED LUO MODEL

The modified Luo model in Eq. (7) was first validated with the existing breakage models for the dimensionless breakage rate (Ω^*), where the superiority of our new breakage model over the existing models was demonstrated. Using the new breakage model, the effect of the turbulence energy dissipation rate and pressure on the breakage frequency was investigated for three liquid systems (water, toluene, and ligroin).

The Zhang model [20] was compared with three sets of experimental data [8,27,34] for the dimensionless breakage rate (Ω^*) with respect to the dimensionless bubble diameter (d^*):

$$\Omega^* = \frac{\Omega}{(1-\alpha_g)n}\left(\frac{\sigma}{\rho_l}\right)^{\frac{2}{5}} \varepsilon^{-\frac{3}{5}} \tag{9}$$

$$d^* = d\left(\frac{\sigma}{\rho_l}\right)^{-\frac{3}{5}} \varepsilon^{\frac{2}{5}} \tag{10}$$

In this study, the three sets of experimental data were also used to validate our modified Luo model in Eq. (7) within $0.5 \le d^* \le 3.5$. The Ω^* obtained from the modified Luo model was compared with those of the Luo [19], Lehr [4], Wang [5], Razzaghi [35], and Zhang [20] models in Fig. 9. The Luo model (1996) and modified Luo model showed a similar trend, but the modified Luo model was more accurate than the Luo model (1996) at high d^*. The Lehr model (2002) under- and overestimated Ω^* at low and high d^*, respectively. The results of both the Wang (2003), Razzaghi (2016)

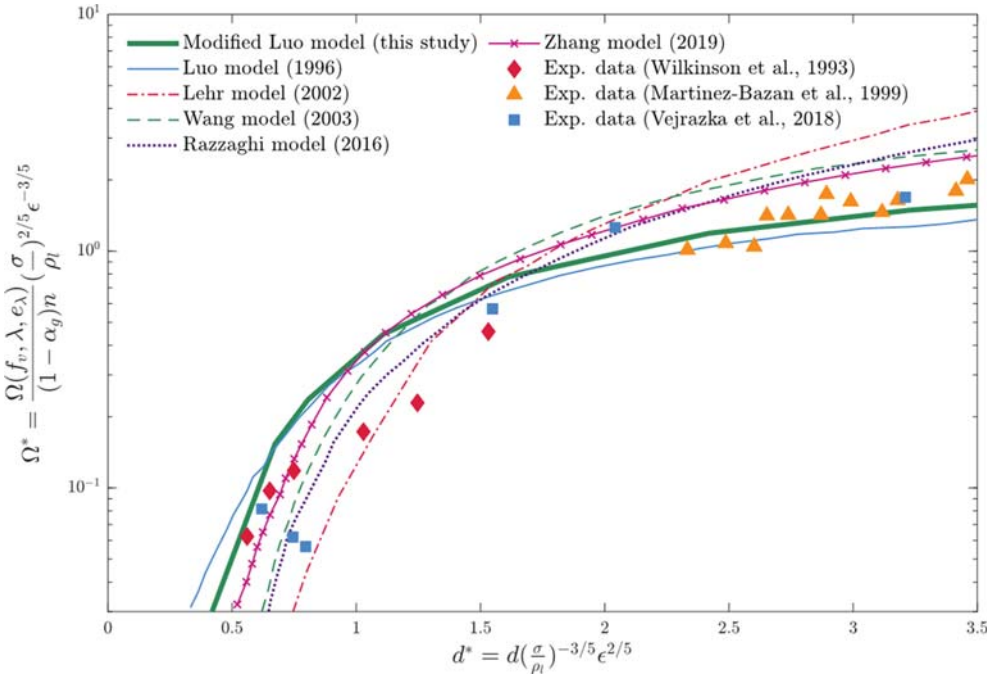

Fig. 9. Comparison of dimensionless breakage rates (Ω^*) with respect to dimensionless bubble diameter (d^*) with experimental data.

Table 3. Average absolute deviation (AAD) and root mean square deviation (RMSD) of modified Luo, Luo, Lehr, Wang, Razzaghi, and Zhang models from experimental data

Model	AAD[a]	RMSD[b]
Modified Luo (this study)	0.19	0.96
Luo (1996)	0.26	1.41
Lehr (2002)	0.90	4.98
Wang (2003)	0.50	2.88
Razzaghi (2016)	0.52	2.87
Zhang (2019)	0.48	2.88

$$^{a}\mathrm{AAD}=\frac{\Sigma_{i=1}^{N_{exp}}\mathrm{abs}(\Omega^*_{exp,\,i}-\Omega^*_{model,\,i})}{N_{exp}},$$

$$^{b}\mathrm{RMSD}=\sqrt{\frac{\Sigma_{i=1}^{N_{exp}}\mathrm{abs}(\Omega^*_{exp,\,i}-\Omega^*_{model,\,i})^2}{N_{exp}}},$$

where N_{exp} is the number of experimental data, and Ω^*_{exp} and Ω^*_{model} are the dimensionless breakage rate obtained from experiments and models, respectively.

and Zhang (2020) models fall between those of the Luo (1996) and Lehr (2002) models, as expected. The Zhang model (2020) showed improved Ω^* over the Wang (2003) and Razzaghi (2016) models, but overpredicted Ω^* at high d^*.

Table 3 reports the average absolute deviation (AAD) and root mean square deviation (RMSD) of the modified Luo, Luo, Lehr, Wang, Razzaghi, and Zhang models from the 24 experimental data. The modified Luo model shows the best fit with the experimental data with the smallest values of the two errors. The deviation of the Luo (1996) model from the experimental data is smaller than that of the Lehr (2002) model. The Wang (2003), Razzaghi (2016), and Zhang (2019) models have similar errors.

Fig. 10 shows the effect of the turbulence energy dissipation rate (ε) and pressure (P) on the breakage frequency (Ω_f) with respect to bubble size (d) for different liquids (water, toluene, and ligroin). In Fig. 10(a), the Ω_f was evaluated for air-liquid systems at P=35 bar under mild turbulent conditions ($0.1\leq\varepsilon\leq10\ m^2/s^3$). As ε increased and surface tension (σ) decreased, the breakage frequency increased, which was also confirmed in the literature [5,19,20]. The Ω_f obtained for toluene and ligroin is approximately two-times greater than that of water over the range of d and ε (see Fig. 10(a)).

In Fig. 10(b), the Ω_f was estimated for air-liquid systems at ε=0.1 m^2/s^3 and $1\leq P\leq35\ m^2/s^3$. The air densities are 1.2, 18, 30, and 42 kg/m^3 at P=1, 15, 25, and 35 bar, respectively. The Ω_f increased by approximately three times when P increased from 1 bar to 35 bar owing to the pressure correction factor in Eq. (7). It is noted that the breakage frequencies at high pressures in Fig. 10 should be further investigated because the pressure correction factor in Eq. (7) was estimated for $1.2\leq\rho_g\leq6\ kg/m^3$ and $4.6\leq d\leq9.8$ mm from experimental data [8].

Table 4 shows the relative computational times of the Luo (1996), Lehr (2002), and Wang (2003) models compared with the modified Luo model (this study) for the evaluation of the breakage rates of water, toluene, and ligroin at d=10 mm, ε=0.1 m^2/s^3, and P=1, 15, and 35 bar. The modified Luo model shows the best performance in terms of computational time. The computational time of the Luo model (1996) is slightly longer than that of the modified Luo model because of more iterations of numerical integrals. The computational time of the Lehr model is approximately two-times longer than that of the modified Luo model. The computational time of the Wang model (2003) is approximately 400-times longer than that of the modified Luo model. Considering that a breakage model is solved in each computational cell and each bubble size

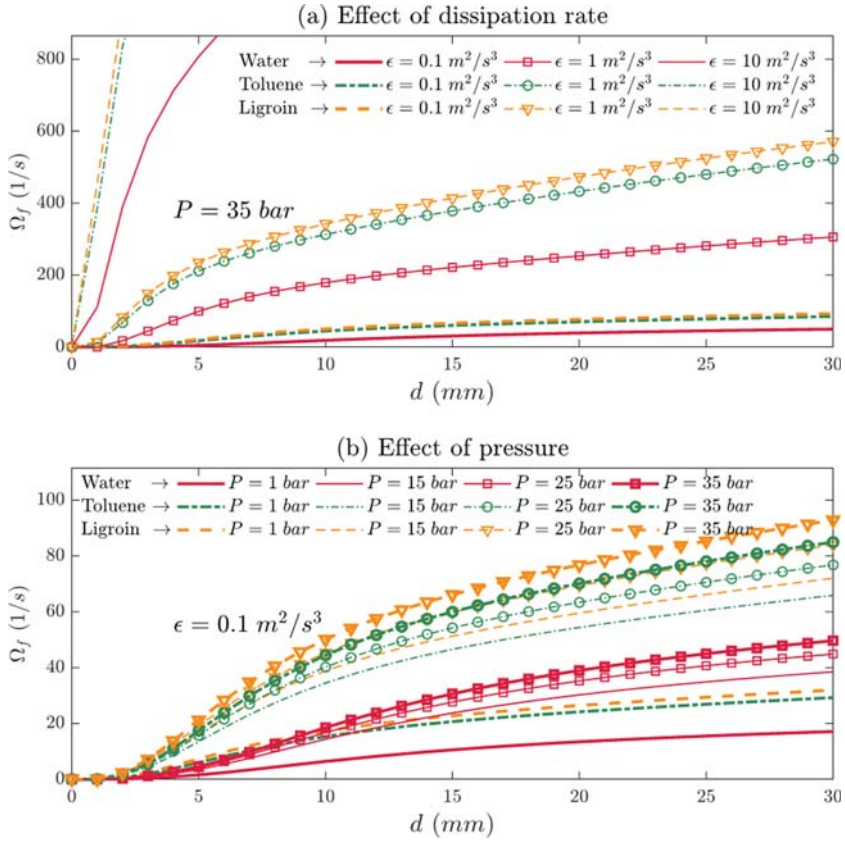

Fig. 10. Effects of turbulence energy dissipation rate (ε) and pressure (P) on breakage frequency (Ω_f) for different liquid properties.

Table 4. Relative computational time for evaluation of breakage rates of water, toluene, and ligroin at d=10 mm, ε=0.1 m^2/s^3, and P=1, 15, and 35 bar

Liquid	P (bar)	Modified Luo model (this study)	Luo model (1996)	Lehr model (2002)	Wang model (2003)
Water	1	1	1.3	5.1	383.4
	15	1	0.8	3.2	242.6
	35	1	1.4	4.7	364.2
Toluene	1	1	2.2	1.6	446.5
	15	1	2.2	1.7	442.7
	35	1	1.9	1.3	356.4
Ligroin	1	1	0.9	1.4	420.1
	15	1	1.1	1.5	441.9
	35	1	0.9	1.4	353.8
Average		1	1.4	2.4	383.5

for CFD with PBM, the computational time is crucial for unsteady CFD simulation in the 2D or 3D geometry. The modified Luo model is applicable to pressurized bubble columns with organic liquids in a computationally-efficient way.

CONCLUSION

Industrial slurry bubble columns are often used for catalytic reactions with organic liquids at high pressure and temperature. However, most bubble breakage models have been developed for ambient conditions in air-water systems. In this paper, a fast and robust breakage model was proposed that is suitable for the homogeneous flow regime and organic liquids at high pressure.

The Luo (1996), Lehr (2002), and Wang (2003) breakage models, which are widely used for the population balance equation (PBE) of bubble columns, were compared in terms of the total breakage rate, daughter size distribution, and computational time. The Luo model was a good candidate in the homogeneous flow regime and was computationally efficient. To consider the effects of pressure and liquid properties on the breakage rate, the Luo model was

modified with four correction factors, which were estimated from experimental data and theoretical breakup rates. The modified Luo model was validated with experimental data for the dimensionless breakup rate. The proposed breakage model showed outstanding computing performance and will be applicable to computational fluid dynamics with PBE for bubble columns. However, the modified Luo model with the four empirical factors can be used for a limited range of physical properties and operating conditions. The model parameters, such as pressure correction factors, should be adjusted for a wide range of operating pressure with reliable hydrodynamic data in the bubble column.

ACKNOWLEDGEMENT

We acknowledge with gratitude the financial support from the R&D Convergence Program of the Ministry of Science, ICT and Future Planning (MSIP) and the National Research Council of Science & Technology (NST) of the Republic of Korea (CRC-14-1-KRICT). This research was also supported by the National Research Foundation of Korea (NRF) grant funded by the Korea Ministry of Science and ICT (Grant number: 2020R1F1A1066097).

NOMENCLATURE

c : breakage time constant [=1/8]
C_f : parameter of surface energy increment [-]
C_d : parameter of surface energy per unit volume [-]
d : mother bubble diameter [m]
d′ : small daughter bubble diameter [m]
d^* : dimensionless bubble diameter [-]
d_c : critical bubble neck diameter [m]
d_{neck} : diameter of the bubble neck [m]
e_λ : kinetic energy of eddy [J]
$e_{\lambda,crit}$: critical kinetic energy of eddy [J]
$\bar{e}_\lambda$: mean kinetic energy of eddy [J]
f_v : bubble breakup volume fraction [-]
k_M : correction factor of breakup rate considering liquid property [-]
k_P : correction factor of breakup rate considering system pressure [-]
Mo : morton number [-]
n : number density of bubbles [$1/m^3$]
n_λ : number density of eddies [$1/m^4$]
P : operating pressure [bar]
P_b : breakup probability density function [-]
P_e : breakup probability density function for eddy [-]
t_b : bubble breakup time [s]
u_λ : turbulent velocity of eddy [m/s]
$\bar{u}_\lambda$: mean turbulent velocity at a distance of d_b [m/s]
$u_{\lambda,crit}$: critical turbulent velocity of eddy [m/s]
We : webber number [-]

Greek Letters

α_g : gas volume fraction [-]
β : daughter size distribution [-]
ε : turbulence energy dissipation rate [m^2/s^3]
λ : bombarding eddy size [m]
λ_{min} : minimum size of eddy [m]
μ_l : liquid viscosity [Pa·s]
ν_l : kinematic viscosity of fluid [m^2/s]
ω_λ : collision frequency density of eddy [$1/m^5/s$]
Ω : total breakage rate [$1/m^3/s$]
Ω_k : breakage rate kernel [$1/m^3/s$]
Ω_f : breakage frequency [1/s]
Ω^* : dimensionless breakage rate [-]
ρ_g : gas density [kg/m^3]
$\rho_{g,0}$: air density at normal condition [=1.2 kg/m^3]
ρ_l : liquid density [kg/m^3]
σ : surface tension [N/m]

REFERENCES

1. B. V. Tran, D. D. Nguyen, S. I. Ngo, Y.-I. Lim, B. Kim, D. H. Lee, K.-S. Go and N.-S. Nho, *AIChE J.*, **65**, e16685 (2019).
2. J. Lee, M. Yasin, S. Park, I. S. Chang, K.-S. Ha, E. Y. Lee, J. Lee and C. Kim, *Korean J. Chem. Eng.*, **32**, 1060 (2015).
3. A. H. Syed, M. Boulet, T. Melchiori and J.-M. Lavoie, *Front. Chem.*, **5**, 68 (2017).
4. F. Lehr, M. Millies and D. Mewes, *AIChE J.*, **48**, 2426 (2002).
5. T. Wang, J. Wang and Y. Jin, *Chem. Eng. Sci.*, **58**, 4629 (2003).
6. H. Im, J. Park and J. W. Lee, *Korean J. Chem. Eng.*, **36**, 1680 (2019).
7. S. Kumar and A. Khanna, *Korean J. Chem. Eng.*, **31**, 1964 (2014).
8. P. M. Wilkinson, A. Van Schayk, J. P. M. Spronken and L. L. van Dierendonck, *Chem. Eng. Sci.*, **48**, 1213 (1993).
9. C. Xing, T. Wang, K. Guo and J. Wang, *AIChE J.*, **61**, 1391 (2015).
10. D. Rudkevitch and A. Macchi, *Can. J. Chem. Eng.*, **86**, 293 (2008).
11. G. Besagni and F. Inzoli, *Flow Meas. Instrum.*, **67**, 55 (2019).
12. C. J. Calderón and J. Ancheyta, *Fuel*, **216**, 852 (2018).
13. P. Yan, H. Jin, G. He, X. Guo, L. Ma, S. Yang and R. Zhang, *Chem. Eng. Sci.*, **199**, 137 (2019).
14. K. Bae, G. S. Go, N. S. Noh, Y.-I. Lim, J. Bae and D. H. Lee, *Chem. Eng. J.*, **386**, 121339 (2020).
15. C. B. Vik, J. Solsvik, M. Hillestad and H. A. Jakobsen, *Comput. Chem. Eng.*, **110**, 115 (2018).
16. P. Chen, M. P. Duduković and J. Sanyal, *AIChE J.*, **51**, 696 (2005).
17. K. Guo, T. Wang, Y. Liu and J. Wang, *Chem. Eng. J.*, **329**, 116 (2017).
18. P. Yan, H. Jin, G. He, X. Guo, L. Ma, S. Yang and R. Zhang, *Chem. Eng. Res. Des.*, **154**, 47 (2020).
19. H. Luo and H. F. Svendsen, *AIChE J.*, **42**, 1225 (1996).
20. H. Zhang, G. Yang, A. Sayyar and T. Wang, *Chem. Eng. J.*, **386**, 121484 (2020).
21. P. Rollbusch, M. Tuinier, M. Becker, M. Ludwig, M. Grünewald and R. Franke, *Chem. Eng. Technol.*, **36**, 1603 (2013).
22. G. Yang, K. Guo and T. Wang, *Chem. Eng. Sci.*, **170**, 251 (2017).
23. M. J. Prince and H. W. Blanch, *AIChE J.*, **36**, 1485 (1990).
24. C. Tsouris and L. L. Tavlarides, *AIChE J.*, **40**, 395 (1994).
25. J. Solsvik, S. Tangen and H. A. Jakobsen, *Rev. Chem. Eng.*, **29**, 241 (2013).
26. G. Grund, A. Schumpe and W. D. Deckwer, *Chem. Eng. Sci.*, **47**, 3509 (1992).
27. C. Martínez-Bazán, J. L. Montañés and J. C. Lasheras, *J. Fluid Mech.*, **401**, 157 (1999).

28. S. Maaß and M. Kraume, *Chem. Eng. Sci.*, **70**, 146 (2012).
29. R. Andersson and B. Andersson, *AIChE J.*, **52**, 2020 (2006).
30. R. P. Hesketh, A. W. Etchells and T. W. F. Russell, *Chem. Eng. Sci.*, **46**, 1 (1991).
31. J. Rodríguez-Rodríguez, C. Martínez-Bazán and J. L. Montañés, *Meas. Sci. Technol.*, **14**, 1328 (2003).
32. D. P. Laurie, *Math. Comput.*, **66**, 1133 (1997).
33. W. Shi, J. Yang, G. Li, X. Yang, Y. Zong and X. Cai, *Chem. Eng. Sci.*, **187**, 391 (2018).
34. J. Vejražka, M. Zedníková and P. Stanovský, *AIChE J.*, **64**, 740 (2018).
35. K. Razzaghi and F. Shahraki, *AIChE J.*, **62**, 4508 (2016).